Powder Technology 397 (2022) 117093

Contents lists available at ScienceDirect

Powder Technology

journal homepage: www.elsevier.com/locate/powtec

Short Communication

Preparation of nano/micro-bimodal Ti/Al/(Mo, W, Cu) powders by simultaneous electrical explosion of dissimilar metal wires

A. Pervikov [a,b,*], K. Suliz [a,b], S. Kazantsev [a,b], N. Rodkevich [b], S. Tarasov [a,b], M. Lerner [a,b]

[a] National Research Tomsk State University, Tomsk, Russia
[b] Institute of Strength Physics and Materials Science SB RAS, Tomsk, Russia

ARTICLE INFO

Article history:
Received 30 September 2021
Received in revised form 22 December 2021
Accepted 23 December 2021
Available online 29 December 2021

Keywords:
Powder
Nanoparticles
Microparticles
Titanium alloys
Aluminum alloys
Exploding wires

ABSTRACT

Novel mixtures of micro- and nanoparticles have been obtained by simultaneous electrical explosion of three intertwisted wires (EEW). The possibility of obtaining of titanium-aluminum micro- and nanoparticles alloyed with molybdenum, tungsten and copper by the electrical explosion of Ti/Al/(Mo, W, Cu – up to 6 at. %) wires has been shown. Spherical particle with sizes from 20 nm to 7 μm are formed under condition of introducing the electric energy at the level of 0.57–0.77 of the total sublimation energy. The mass content of particles with sizes less than 100 nm does not exceed 10%. The phase composition of powders includes double and triple intermetallic phases, titanium oxide (TiO) as well as phases of the initial metals. The study of the phase composition of bulk materials obtained by sintering powders Ti-Al-Mo, Ti-Al-W and Ti-Al-Cu for 2 h at 1000 °C showed the increase in the content of intermetallic phases, providing enhanced physical and mechanical properties of the titanium-aluminum alloys. The results of the studies show that the obtained powders alloys can be used to produce feedstocks of TiAl alloys.

1. Introduction

Development of processes intended for fabrication of figurine-shaped components from heavily filled 40–60 vol% polymers (granulated or filament feedstocks) is a relevant objective in modern materials science and industry [1]. The above-mentioned processes include feedstock extrusion [2,3] and injection [4,5] of powder fillers such as copper [6], stainless steel 316 L [7], magnesium alloy AZ91 [8], oxides [9], and cemented carbides [10,11]. Titanium-based feedstocks are to become of great demand now for fabricating, for example, intermetallic compound (IMC) TiAl that is widely used in automobile and aircraft industries as well as in medicine [12–14].

Fluidity is a key characteristic of the feedstock performance and it is determined by characteristics such as the chemical nature of the binder used [15] and particle size distribution [16]. It was shown [17] that fluidity improved when the feedstock was prepared by blending together micron- and nanosized particles. Such an approach allowed also to reduce the sintering temperature and thus improve the physic-mechanical characteristics of the articles sintered [18]. These results can be evidence in favor of further efforts to be undertaken for obtaining high-fluidity homogeneous feedstocks by intermixing micro- and nanosized metallic particles.

A promising process for fabrication of such micro/nano particle mixtures can be electric explosion of wires (EEW), which is a single stage one that allows producing spherical particles with the desired particle size distribution in the range of 10^{-8} to 10^{-5} m [19]. Other advantages of this process include low power consumption at the level of 25–50 kW/h × kg and controlled buffer gas composition which allows adjusting both dispersion and phase composition of the particles produced [20,21].

The first use of EEW for fabricating homogeneous micro/nano particle mixtures by the example of Ti/Al particles was reported [22] when intertwisted Ti and Al wires were exploded and allowed obtaining spherical particles of various phase compositions and size distributions for the benefit of improving both feedstock fluidity and sintered sample characteristics [23–25].

The results of investigations obtained in this field allow observing that higher functional characteristics of the TiAl IMCs can be achieved by extra alloying them with other metals [26,27], for instance, adding 3 at.% of Fe and Co improved both mechanical strength and plasticity characteristics of the TiAl [28]. Alloying the TiAl with 3 to 15 wt% Mo resulted in improved strength and corrosion resistance [29], while adding W and Mo resulted in higher heat resistance and high-temperature strength [30].

The above-discussed results enabled us to make it the objective of this work to:

* Corresponding author at: National Research Tomsk State University, Tomsk, Russia.
E-mail address: pervikov@list.ru (A. Pervikov).

https://doi.org/10.1016/j.powtec.2021.117093
0032-5910/

- EEW produce TiAl micro/nano particles alloyed with Mo, W, and Cu from three intertwisted wires, characterize then for particle size distribution and phases.

- Form green samples and sinter them to obtain bulk samples with phases to provide the desired level of functional characteristics.

Using both W and Mo for alloying the TiAl can be justified by the necessity of attaining higher heat resistance and high-temperature strength to the figurine-shaped articles produced by extrusion of powder feedstock with the following removal of polymer binder and sintering the micro/nano particles.

Copper is a good alloying element to improve the plasticity of Al_3Ti-based TiAl alloy, which usually provide high heat resistance but low plasticity [31]. The results of this work may be then used for developing TiAl micro/nano feedstocks.

2. Experimental

2.1. Preparation of powders

Ti/Al/(Mo, W, Cu) micro- and nanoparticles were prepared using an EEW machine as previously reported elsewhere [21]. The energy (E(t)) and temporal characteristics of the simultaneous EEW on three intertwisted wires of dissimilar metals as shown in Table 1 were determined from corresponding time dependences of current (I(t)) and voltage (U(t)) recorded using an ohmic voltage divider, a current shunt and a digital oscilloscope [23]. The EEW parameters are given in Table 1, where d_w is the wire diameter of the, l_w is wire length, N is the mass fraction of metal in the products of the simultaneous EEW, C is the electric capacity of the capacitor bank, U_0 is the charging voltage of the capacitor bank, E_s is the sublimation energy of the metal, P is the pressure of the buffer gas (argon, 0.3 MPa). To calculate the E/E_s parameter, the magnitude of E was determined from experimental data plotted in Fig. 2, Fig. 5 and Fig. 8. The magnitude of E_s was calculated as algebraic sum of sublimation energies of corresponding wire metals ($\sum E_s$) from Table 1. The frequency of wire explosions was 0.3 Hz, and the mass of the powder samples prepared was 200 g. Upon the preparation, the powder samples were passivated with atmospheric oxygen for 48 h to prevent spontaneous ignition when working.

2.2. Characterization of powders

Particle size distribution was determined by sedimentation analysis using a disc centrifuge CPS DC24000 as follows. A powder load of 0.020 ± 0.002 g was placed into 10 mL of distilled water and sonicated there for 1 min. A 0.1 mL aliquot was then sampled and examined for particle size distribution using particle population not less than 5.0–6.0 10^9 particles.

The particle micrographs and EDS element distribution maps were obtained using a scanning electron microscope (SEM) «LEO EVO 50» (Zeiss, Germany) and transmission electron microscope JEOL JEM-2100 (Tokyo Boeki Ltd., Japan).

Table 1
Parameters of the Ti/Al/Me (Mo, W, Cu) simultaneous EEW.

Sample	Metal	d_w, mm	l_w, mm	N, wt%	C, μF	U_0, kV	E_s, J	P, MPa
Ti-Al-Mo	Ti	0.30	80	60	1.6	22	252	0.3
	Al	0.25		25			130	
	Mo	0.10		15			44	
Ti-Al-W	Ti	0.30	80	44	2.4	21	252	
	Al	0.35		35			255	
	W	0.10		21			34	
Ti-Al-Cu	Ti	0.30	80	42	3.2	20	252	
	Al	0.42		49			366	
	Cu	0.10		9			30	

The phase compositions of the powder and sintered sampled were determined using an XRD-6000 diffractometer (Shimadzu, Kyoto, Japan), CuKα radiation. The data obtained were processed using XPowder CELL 2.4 ver.2004 software package.

2.3. Preparation of bulk samples

The temperature/time diagram in Figure shows a regime applied for sintering all three powder compositions Ti/Al/Me (Mo, W, Cu).

The pre-pressed green samples were held for in a chamber with residual pressure of 1 Pa at 200 °C for 2 h in order to remove the gas adsorbed on the surface of the particles. Then, the samples were sintered at 1000 °C for 2 h. All samples had the following geometric dimensions after pressing: diameter 20.0 ± 0.25 mm, height 4.0 ± 0.15 mm. The masses of the sintered TiAlMo and TiAlW samples were 4 g, TiAlCu - 3 g.

3. Results

3.1. Ti-Al-Mo powder

Fig. 2a shows the I(t), U(t) and E(t) curves typical for the simultaneous triple Ti/Al/Mo wire EEW. Time dependence of I(t) shows that the mode of simultaneous Ti/Al/Mo EEW is close to that of low rate energy release and low efficiency [32]. The ratio of the energy input into the wires E to the total sublimation energy E_s of titanium, aluminum, and molybdenum wires was assumed as 0.66. It should be noted that due to the lower electrical resistivity of aluminum in comparison with titanium and molybdenum, the $E/\sum E_s$ value for the aluminum would be greater than the total value of 0.66. It was earlier established by the example of dual Ti/Al wire explosion at $E/\sum E_s \approx 0.85$, 1.25, and 1.48 that values of E/E_s for Ti and Al wires had approximate magnitudes 0.70, 1.0, 1.16 and 1.0, 1.52, 1.84, respectively [22]. These data show that in combined explosion of three wires such as Ti/Al/Mo, the E/E_s magnitudes would be less 0.66, i.e. the mean value. At $E/\sum E_s \approx 0.66$, the most of the expanding Ti/Al/Mo EEW products will be a mixture of micron and submicron droplets of liquid metals such as Ti, Mo, and Al. The existence of the above-described phase state of the Ti/Al/Mo EEW products is determined by previously established relationships between the $E/\sum E_s$ value and the phase state of the expanding EEW products [33,34].

Particle size distribution and corresponding mass/size distribution are shown in Fig. 2b, c, respectively. According to Fig. 2c the number average size of Ti-Al-Mo particles is in the range 30–40 nm. The mass

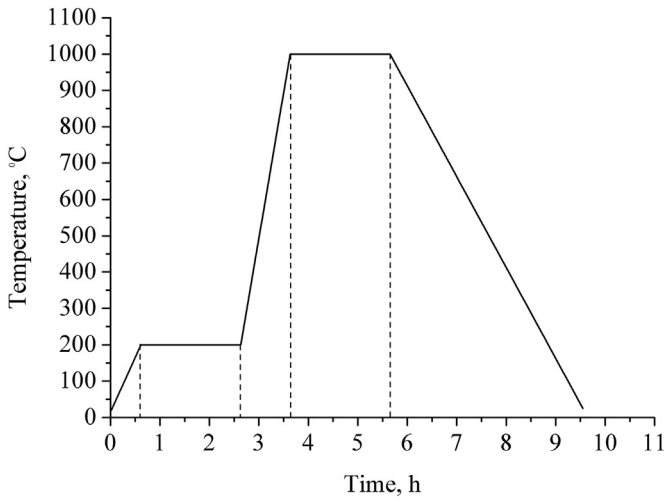

Fig. 1. Processing scheme for the sintering of pressed Ti/Al/Me (Mo, W, Cu) samples.

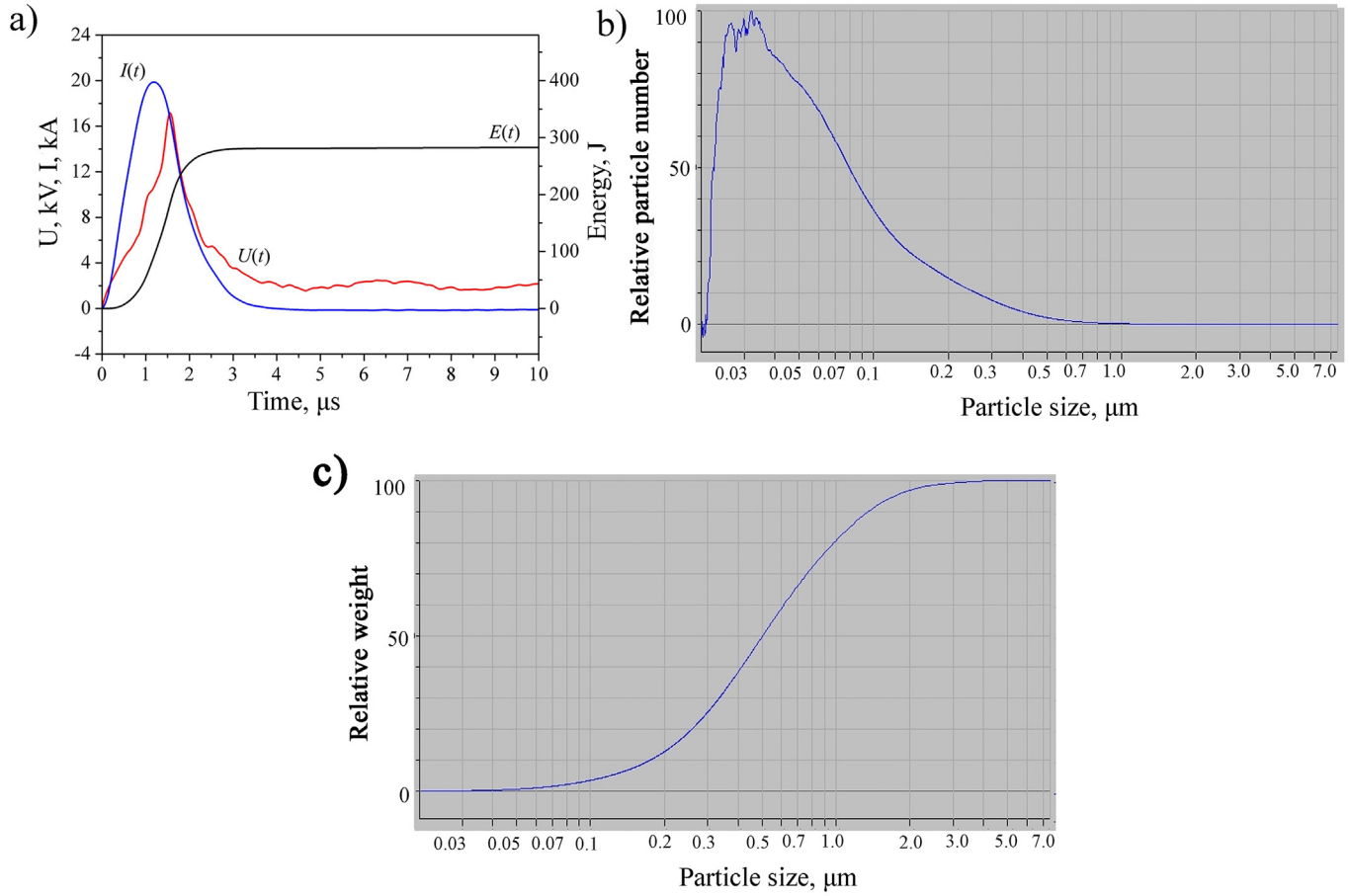

Fig. 2. Time dependencies of I(t), U(t) and E(t) for the simultaneous Ti/Al/Mo EEW (a), particle size distribution (b) and cumulative mass/size distribution (c).

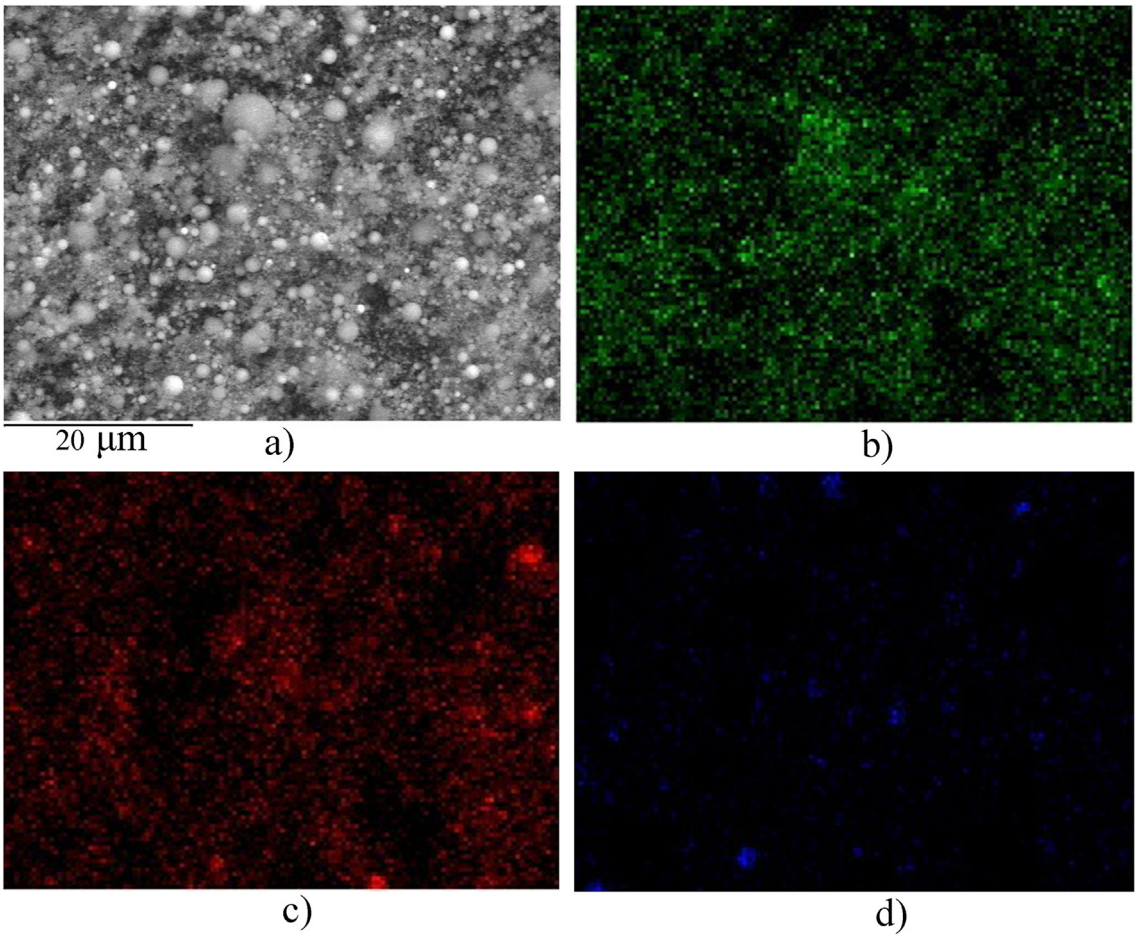

Fig. 3. SEM image of the Ti/Al/Mo particles (a) and EDS element distribution maps of titanium (b), aluminum (c) and molybdenum (d).

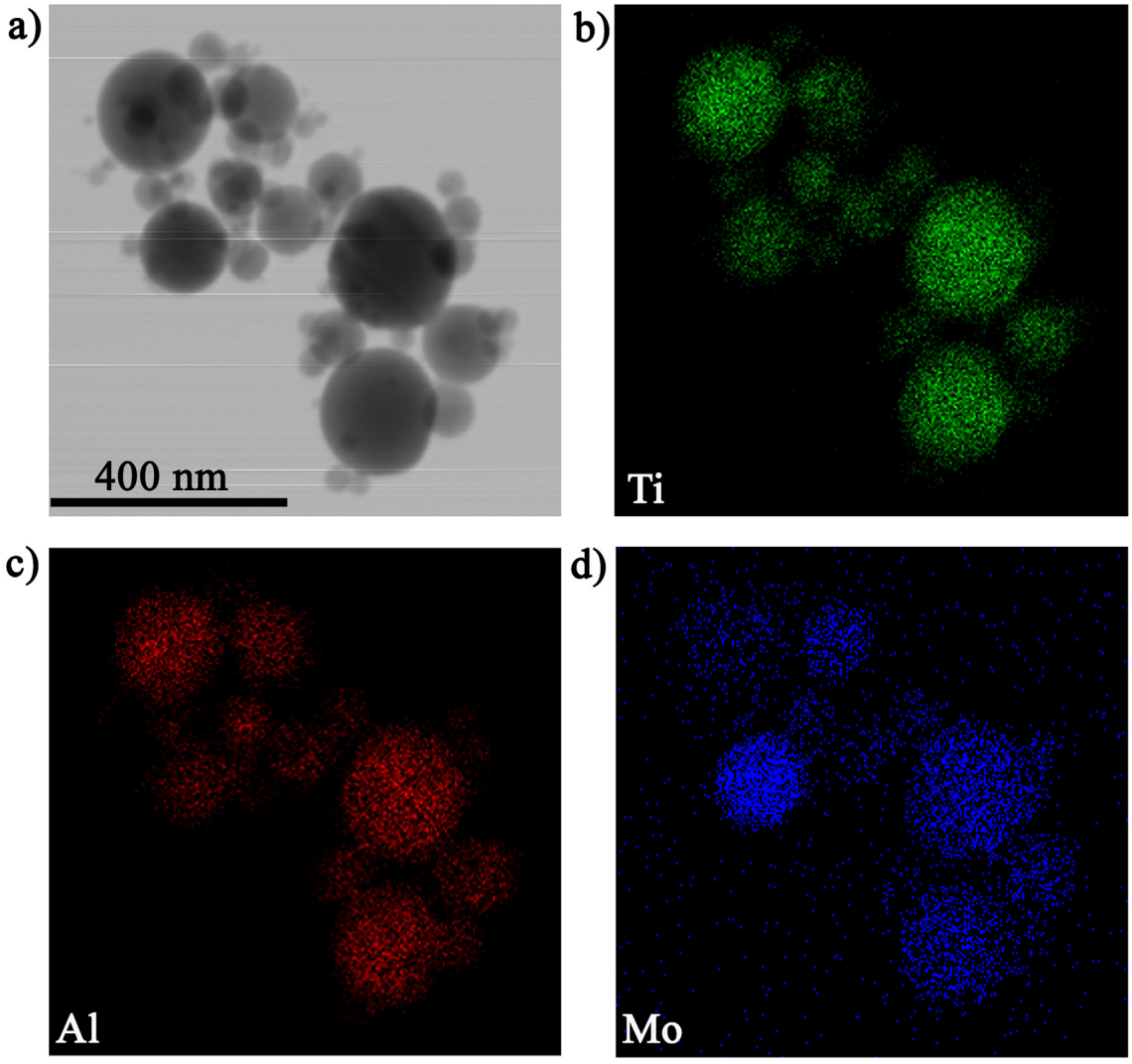

Fig. 4. TEM image of the Ti/Al/Mo particles (a) and elemental distribution maps of titanium (b), aluminum (c) and molybdenum (d).

distribution curve in Fig. 2c allows observing that the mass fraction of particles with sizes below 100 nm is not higher 5 wt%. The mass fraction of micron-sized particles is about 20 wt%.

Fig. 3a shows an SEM BSE image of the particles and EDS element distribution maps (3b-3d). The EDS data allow observing the homogeneous distribution of elements over the probe area. At the same time,

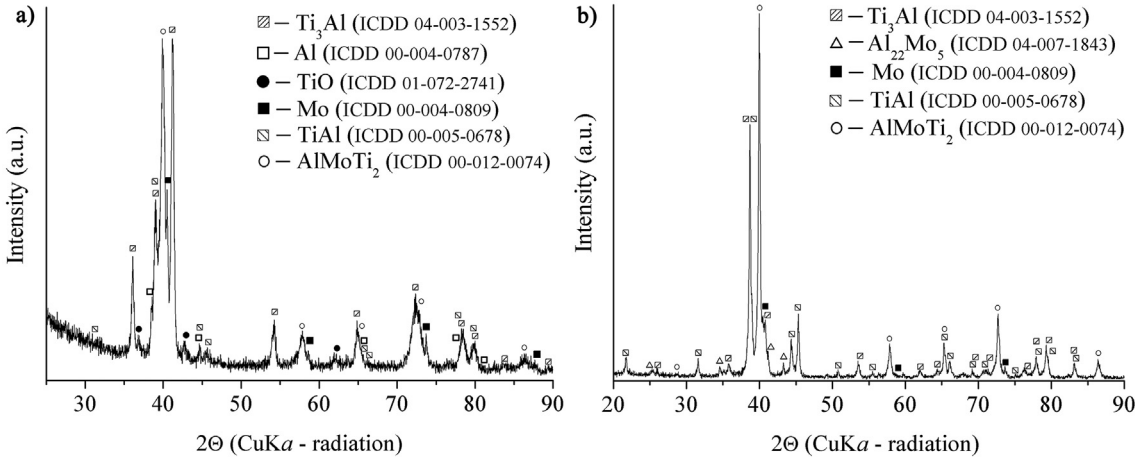

Fig. 5. XRD patterns of the Ti-Al-Mo as-exploded powder (a) and as-sintered sample (b).

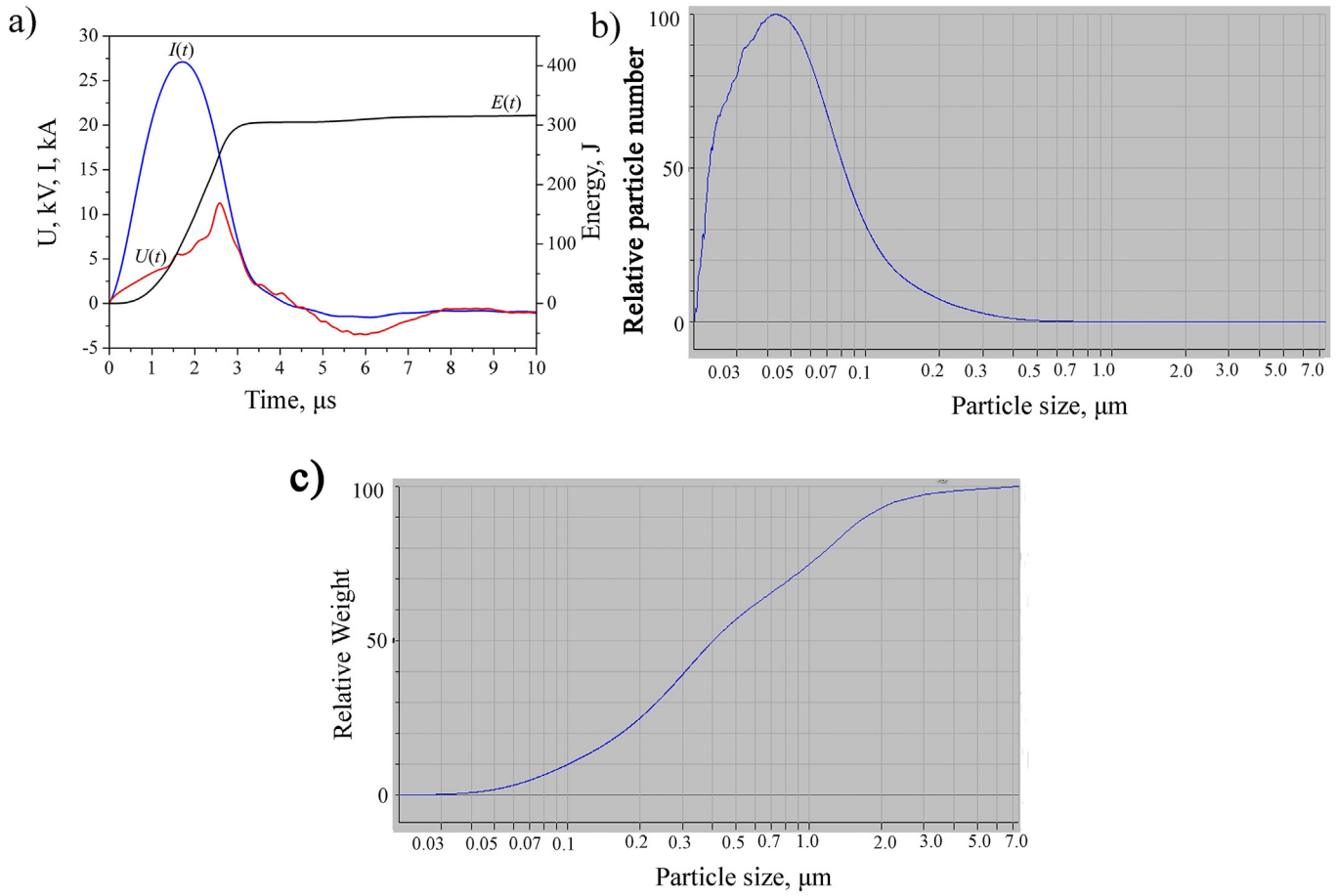

Fig. 6. Time dependencies of I(t), U(t) and E(t) for the simultaneous Ti/Al/W EEW (a). Particle size distribution (b) and cumulative mass/size distribution (c).

micron-sized particles of initial metals are also present in the sample. The presented data show that the SEM results relating to particle size and element composition of the Ti-Al-Mo powder are really those that determined by the energy parameters of the EEW process of Ti-Al-Mo wires.

Despite low *E/Es* values inherent in both Mo and Ti wires the EDS data show the presence of both Mo and Ti in the nano-sized Ti-Al-Mo particles (Fig. 4).

Fig. 5 shows the XRD patterns of both as-exploded Ti-Al-Mo powder and as-sintered bulk sample. The XRD analysis revealed a multiphase composition of the Ti-Al-Mo powder, which included intermetallic compounds (IMC), free metals and oxides. Sintering of the pre-pressed samples having a relative density of about 75% resulted in the formation of $Al_{22}Mo_5$ phase and the absence of TiO phase (Fig. 5a). The absence of TiO is probably due to the fragmentation of the surface oxide layer to X-ray amorphous state during sintering. The sintering of the powder lead to increasing the content of the $AlMoTi_2$ IMC, which provided improving heat resistance and high temperature strength of titanium-aluminum alloys [35,36].

3.2. Ti-Al-W powder

Fig. 6a shows the I(t), U(t) and E(t) curves that were in-situ obtained during EEW on Ti/Al/W intertwisted wires. The shape of the I(t) curve demonstrates that simultaneous EEW of Ti/Al/W wires occurred with low energy release rate and low efficiency. The ratio of the energy input into the wires (E) to the total sublimation energy of titanium, aluminum and tungsten can be assumed as 0.57 from the considerations as follows. Tungsten, as well as molybdenum, possesses high specific electric resistance and high melting point that are limiting factors for energy input by passing a current pulse through a wire. In connection with this, the E/E_s values used for EEW on tungsten and titanium wires must be less than the mean value 0.57. This value shows that the most part of expanding products obtained by EEW on Ti/Al/W would be a mixture of micron- and submicron-sized droplets of liquid Ti, W and Al metals.

Both particle size and mass/size distributions obtained from EEW on triple *Ti-Al-W wire* system are shown in Fig. 6b and Fig. 6c, respectively. The number average particles size is within the range 40–50 nm. The mass fraction of particles with the sizes below 100 nm is about 25 wt% (Fig. 6c).

Fig. 7 shows the SEM BSE image of the particles and EDS element distribution maps (7b-7d). The EDS maps demonstrate almost homogeneous distribution of elements over the probe area. Micron-sized particles of the initial metals are also present in the sample. The presented data show that the dispersion and EDS element composition of the Ti/Al/W powder are consistent with those determined by energy parameters of the Ti/Al/W EEW.

EDS data show the presence of both W and Ti in the nano-sized Ti-Al-W particles (Fig. 8b, d). It should be noted that the contents of both elements in the nano-sized particles would be always less than those in the explosion products by quantities of those contained in the micron-sized particles. Increasing the $E/\sum E_s$ would allow reducing the mass content of both micron-and submicron-sized Mo, W and Ti droplets in the expanding explosion products and thus homogenizing both phase and element compositions of EEW particles.

XRD patterns of the Ti/Al/W powder and the bulk sample obtained by vacuum sintering of the powder (Fig. 9) in accordance

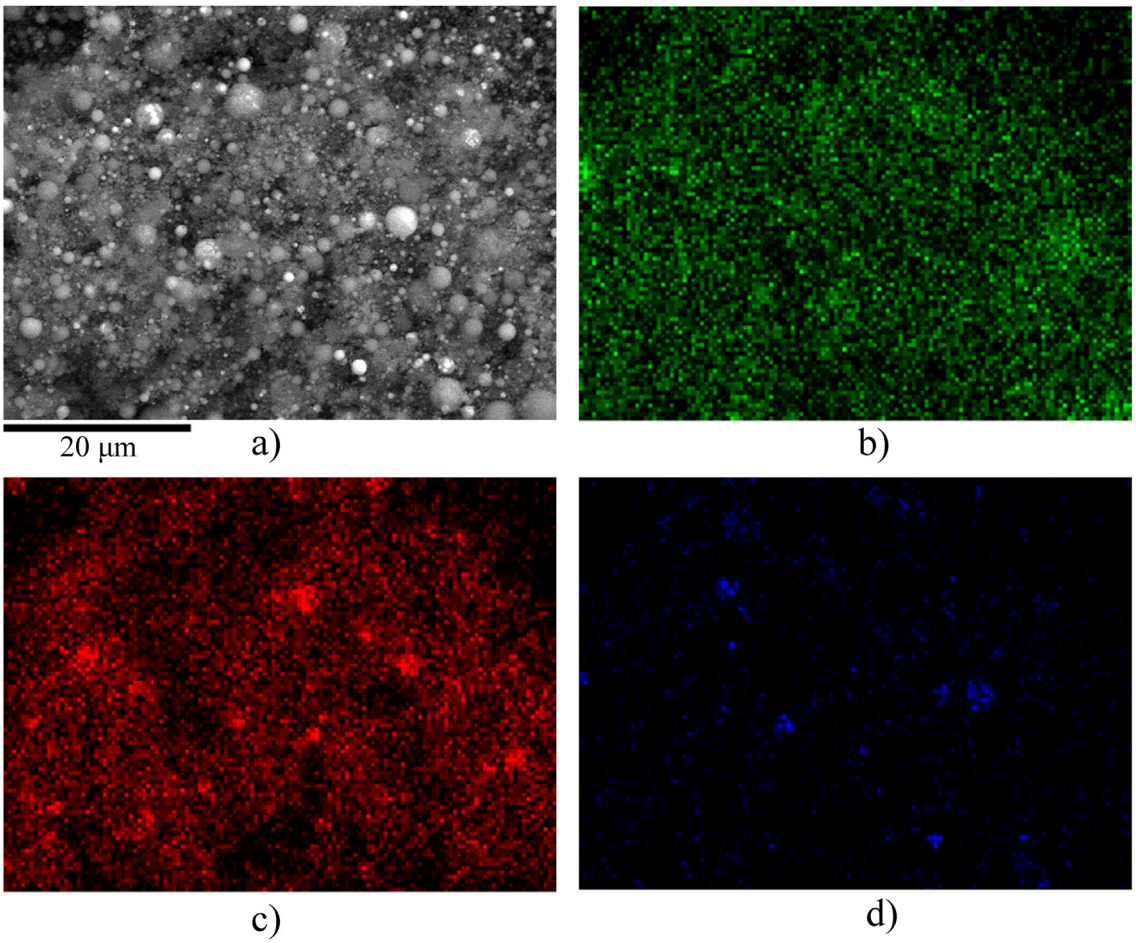

Fig. 7. SEM BSE image of the Ti/Al/W particles (a) and EDS maps of titanium (b), aluminum (c) and tungsten (d).

with the processing scheme presented in Fig. 1. The XRD on Ti/Al/W powder shows a multiphase composition including IMCs, metal and oxide phases. The sintering of pre-pressed to the relative density ~ 70% samples resulted in the formation of Al_2Ti IMC without any TiO (Fig. 9b).

3.3. Ti-Al-cu powder

The I(t), U(t) and E(t) curves were in-situ obtained during EEW on Ti/Al/Cu intertwisted wires (Fig. 10a) to characterize the EEW. The shape of the I(t) curve testified that EEW of triple Ti/Al/Cu system occurred with low energy release rate and low efficiency. The ratio of the energy input into the wires (E) to the total sublimation energy of titanium, aluminum and copper was 0.77. During the EEW both copper and aluminum wires had their electrical resistivity values lower than that of titanium so that the energy input into the two wires was higher than the mean value of 0.77. Particle size and mass distributions in Fig. 10b, c allow observing that the number average size and mass fraction of Ti-Al-Cu particles smaller than 100 nm were 48–50 nm and 10 wt%, respectively. The micron-sized particles composed the mass fraction about 18 wt%.

SEM BSE image (Fig. 11a) of the particles and EDS (Figs. 11b-11d) allow observing micron-sized particles of titanium and aluminum and close to homogeneous distribution of elements over the area of interest. The absence of micron-sized copper particles is due to the low specific electrical resistance of the copper, which provides the energy input sufficient for evaporation of copper thus giving a minimum content of micron-sized droplets of liquid metal [33]. The presented data show that both particle size and element composition of Ti/Al/Cu powder are consistent with the energy parameters of Ti/Al/Cu EEW.

XRD patterns of the Ti/Al/Cu powder (Fig. 12a) and the bulk sintered sample (Fig. 12b) show that Ti/Al/Cu powder is of a multiphase composition, including IMCs, metal and oxide phases (Fig. 12a) while sintering of pre-pressed to relative density of about 72% samples resulted in disappearance of TiO and Cu_3Ti phases. After sintering the predominant phase is $Al_{0.67}Cu_{0.08}Ti_{0.25}$, which provides titanium-aluminum alloys with improved mechanical properties [31].

4. Discussion

The results of the studies show that electrical explosion of Ti/Al/Me (Mo, W, Cu) triple wire system at $E/E_s < 1$ allowed obtaining a powder mixture consisting of micro- and nanoparticles with sizes varying from 20 nm to 7 μm. The phases detected in the particles allow concluding that the mechanism of the particle phase formation at $E/E_s < 1$ differs significantly from that of at $E/E_s > 1.0$ [24,25].

At $E/E_s > 1$ electric explosion of a wire is accompanied by overheat instabilities [37] so that the explosion products can be identified as a mixture of nanosized liquid metal clusters and weakly-ionized plasma. Full gas-plasma state of the products was not achieved even at $E/E_s =$ 2–3 [38,39] and only extra heating of the products during the arc discharge stage might result in full evaporation of the clusters and transition to the gas-plasma state [40–42].

It was mentioned above that magneto-hydrodynamic instabilities develop during EEW at $E/E_s < 1$ [43] that results in forming a mixture of micron - and submicron-sized liquid droplets with weakly ionized

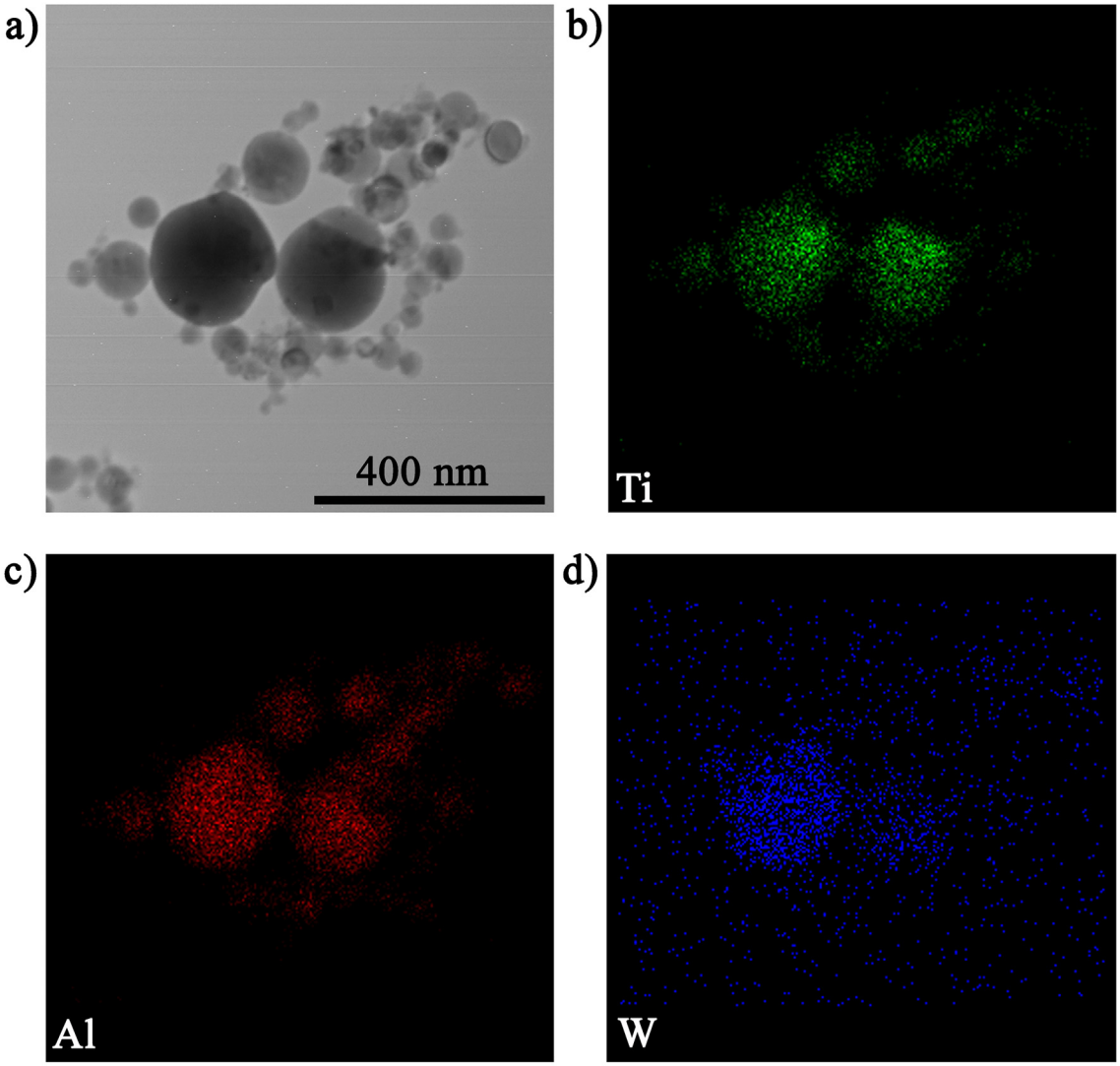

Fig. 8. TEM image of the Ti/Al/Mo particles (a) and elemental distribution maps of titanium (b), aluminum (c) and tungsten (d).

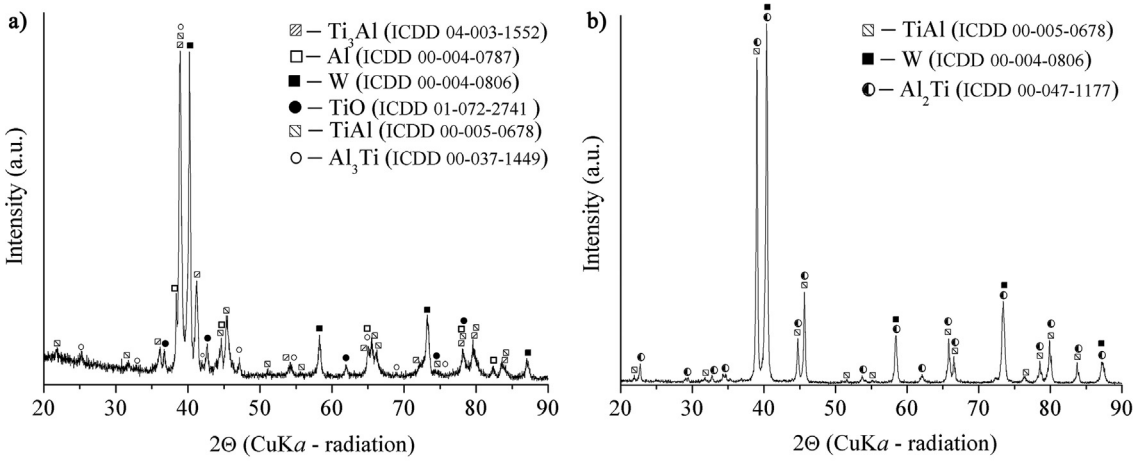

Fig. 9. XRD patterns of the Ti/Al/W powder (a) and sintered sample (b).

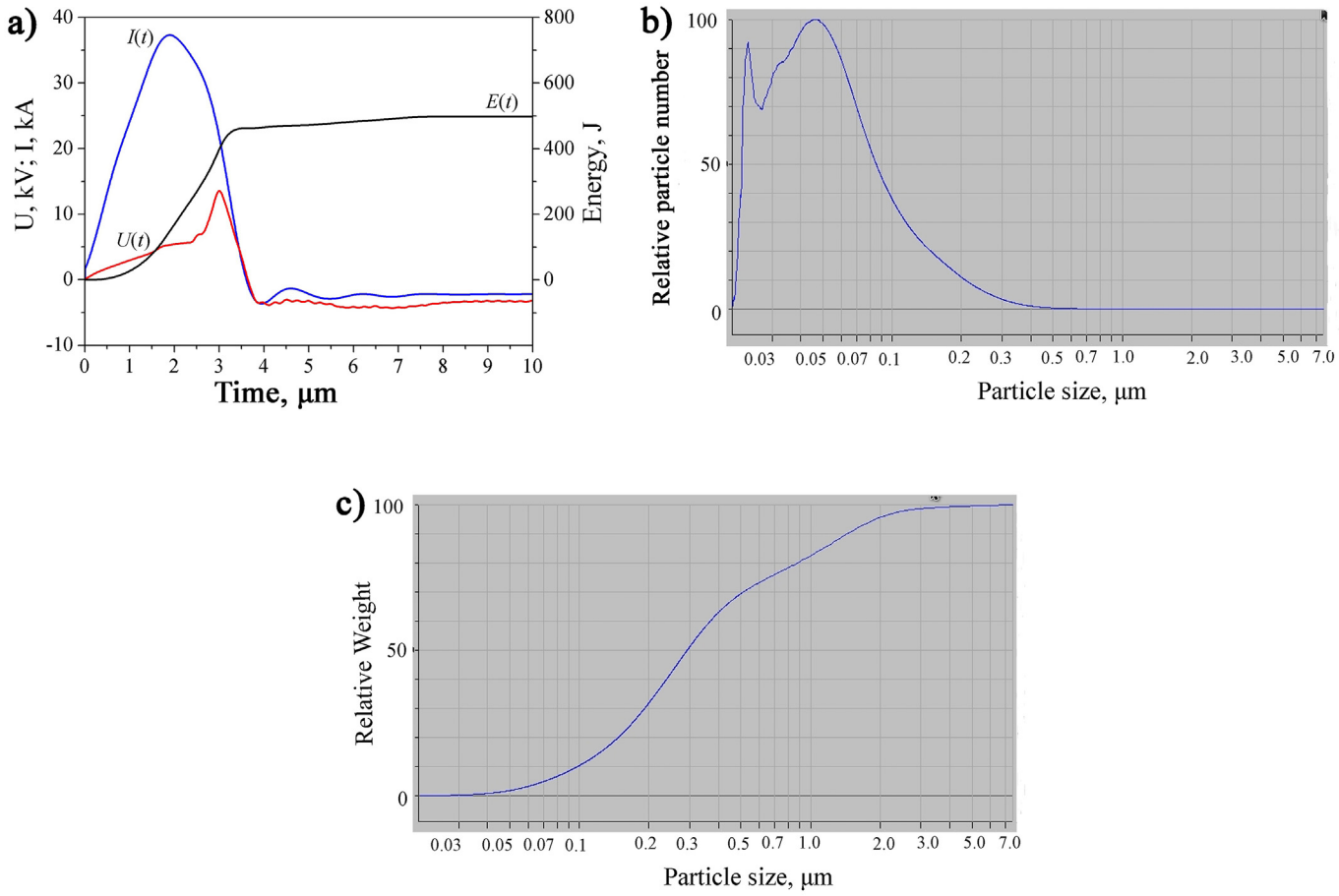

Fig. 10. Temporal dependencies of I(t), U(t) and E(t) for the simultaneous Ti/Al/Cu EEW (a) particle size distribution (b) and cumulative mass vs.size distribution (c).

plasma. Using even lower threshold $E/E_s \approx 0.2–0.3$ ratio may give the droplets of their sizes larger the wire diameter [44].

In case of EEW on triple intertwisted dissimilar metal wires at $E/\sum E_s \approx 0.2–1.0$, both particle size and mass distributions depend on the specific electric resistances of the wire metals. When intertwisted, all the wires form a parallel circuit so that the current amplitudes are in reverse proportion to the specific resistances of the corresponding metals [23] and in accordance to the Joule-Lenz law the most intense heating occurs in a wire with the maximum current ($E_w \approx I^2$). Under such a condition, the E_w/E_s ratio for Cu or Al would be always higher than that of for Ti, Mo, or W. The same would be true for average $E/\sum E_s$ ratio.

Both mass fraction and size of micron-sized droplets decrease when increasing the E_w/E_s, therefore, the maximum mass fraction of micro-sized droplets (with respect to the wire mass) in Ti/Al/Me (Mo, W, Cu) explosion products would be for Mo and W.

The results obtained in this work allow concluding that using $E/\sum E_s > 0.6$. for EEW of two and more dissimilar metals with negative enthalpies of mixing ($\Delta H_{mix} < 0$) is the most favorable approach because of reducing amount of micron-sized particles. The presence of these particles is detrimental from the viewpoint of future structural and mechanical characteristics of compacted components.

Compaction and sintering of powders of metals with high negative ΔH_{mix} (Ti–Al, Ni–Al, Co–Al et al) values can be accompanied by evaporation and formation of gas pores during self-propagating high-temperature synthesis (SHS) [45]. In connection with this, micron-sized particles of these metals distributed in powders would hardly contact each other during sintering. Therefore, minimum $E/\sum E_s$ values may be varied in some ranges in EEW of two or more wires of metals with $\Delta H_{mix} > 0$ to provide the desired balance of micro- and nano-sized particles and thus tailor the compacted material characteristics.

Using the maximum $E/\sum E_s$ values for EEW of metals with $\Delta H_{mix} < 0$ and $\Delta H_{mix} > 0$ will cause obtaining the maximum content of nano-sized particles, which almost will have no effect on the feedstock fluidity and physico-mechanical characteristics of the sintered samples. These maximum $E/\sum E_s$ values will be individually determined for each specific dissimilar metal wire system.

The E/E_s values may be varied in the range 0.3 to 1.0 to adjust the contents of EEW micro- and nano-sized particles and thus obtain feedstocks with desired characterisitcs [46].

The presence of intermetallic and metal phases in the powders is due to the heterophase state of the expanding EEW products. The expansion of the EEW products is an adiabatic process. As a result of this expansion, the micron sized droplets of liquid metal and vapor/plasma cool inhomogeneously. The micron-sized metal droplets, which have a larger mass, take more time to solidify. When cooling, electrons are emitted from the surface of hot liquid metal droplets, so that the micron particles acquire positive electric charge. Formation of nanoscale negatively charged particles occurs as a result of the deposition from the vapor phase.

The Coulomb interaction between positively and negatively charged particles provides formation of a homogeneous mixture of micro- and nanoparticles [47] so that nano-sized Al-rich particles deposit on the surfaces of hot micron-and submicron-sized ones. Because of such an interaction in binary systems with negative value of the enthalpy of mixing, metal diffusion occurs with the formation of an alloy. Table 2 summarizes the values of the mixing enthalpy of metals in accordance with the Miedema model [48]. Analysis of the presented data shows

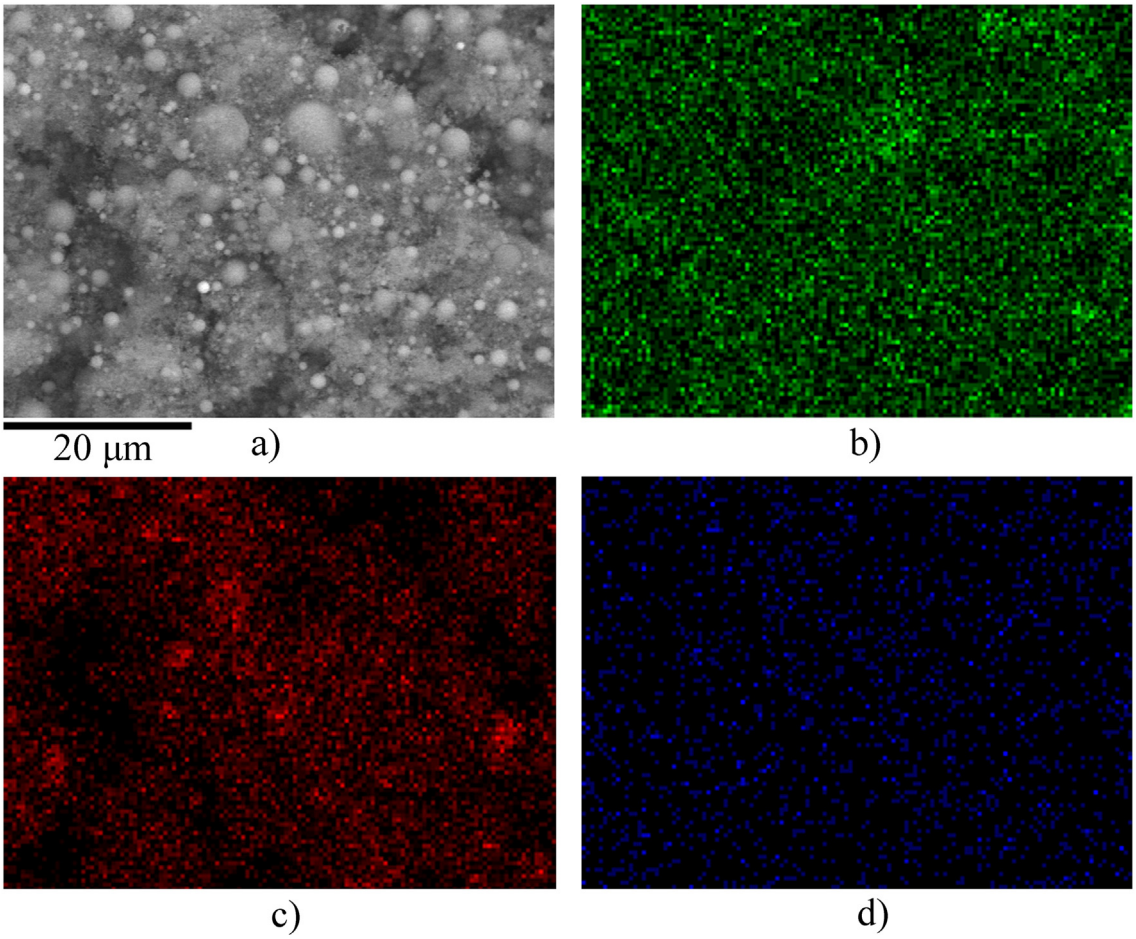

Fig. 11. SEM image of the Ti/Al/Cu particles (a) and elemental distribution maps of titanium (b), aluminum (c) and copper (d).

that for the selected ternary systems, the formation of Ti–Al alloys is predominant.

Ti–Al alloy is formed because of the deposition of aluminum nanoparticles on the surface of the titanium ones and subsequent mutual diffusion. The enrichment of the surface of titanium particles with aluminum prevents oxidation of titanium [49]. However, the TiO phase was present in all powder samples. The presence of this phase, in our opinion, is due to the fact that there is no continuous IMC Ti_xAl_y protective layer on the surface of titanium microparticles.

The problem of metal oxide formation in powders obtained by EEW can be solved by placing the powder in a passivating liquid to prevent their contacting with air. This approach was demonstrated by the example of copper nanoparticles placed in an $AgNO_3$ solution [50]. Various organic solvents can be used as a passivation medium when preparing the EEW powder feedstocks [15]. Another approach was to reduce the content of TiO phase in the powder by increasing the energy *E* input into the wires. Increasing *E* contributes to reduction of both mass content and size of the micron-sized droplets. With the decrease in the

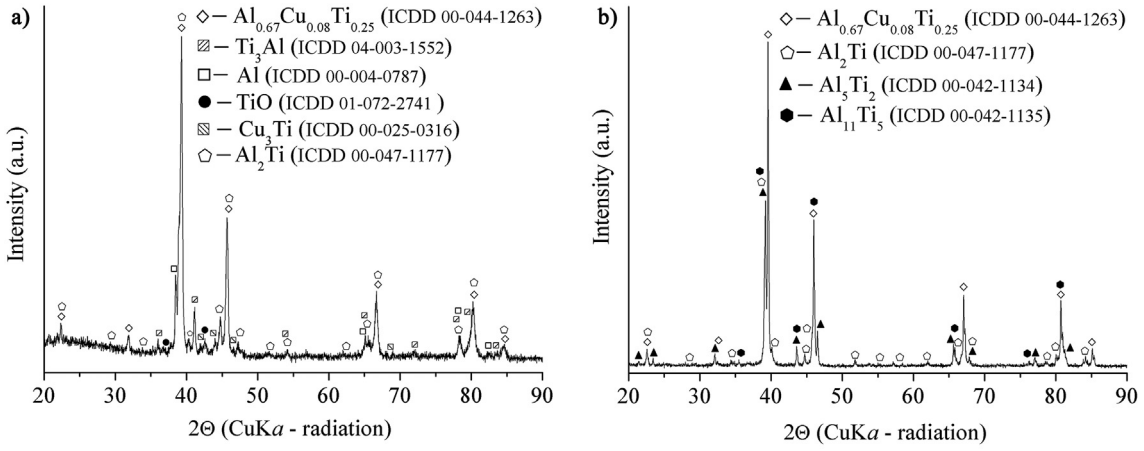

Fig. 12. XRD patterns of the Ti/Al/Cu powder (a) and sintered sample (b).

Table 2
Molar enthalpies of mixing of binary systems (kJ/mol).

Metals	Ti	Al	Mo	W	Cu
Ti	–	−40.5	−3.5	−5.6	−8.8
Al	–	–	−16.6	−13.8	−10.5
Mo	–	–	–	−0.2	18.4
W	–	–	–	–	22.4
Cu	–	–	–	–	–

size of titanium droplets the conditions for the formation of a protective Ti_xAl_y IMC layer are established.

The presence of a third alloying element in the explosion products provides conditions for the formation of ternary IMCs as such as $AlMoTi_2$ and $Al_{0.67}Cu_{0.08}Ti_{0.25}$ IMCs. However, Ti/Al/W system did not contain any ternary IMCs. Both theoretical and experimental studies show that substitution of tungsten atoms by titanium or aluminum ones allows increasing the strength of titanium-aluminum alloys and their resistance to oxidation [51,52]. The XRD study of the bulk samples show that sintering provides formation of the ternary phases thus providing the necessary functional properties of titanium-aluminum alloys. It should be noted that the formation of the necessary structural-phase state in sintered samples Ti/Al/(Mo, W, Cu) from the EEW powders requires additional research to establish the regularities between the dispersion, phase composition of powders, sintering temperature and dwelling time and density, structure of the obtained alloys.

5. Conclusion

For the first time titanium-aluminum powder alloyed with a third metal has been prepared by EEW method. The investigation in particle size distribution and phase composition of powders prepared showed that the energy input into the wires in the range (0.57–0.77) E_s, provides formation of the particles with sizes varying from 20 nm to 7 μm. Mass content of particles with sizes less than 100 nm does not exceed 10%. The phase composition of powders includes IMCs which may attribute enhanced functional properties to the titanium-aluminum alloys.

Phase content analysis in the sintered Ti-Al-Mo and Ti-Al-Cu samples showed that sintering resulted in increased contents of IMCs such as $AlMoTi_2$ and $Al_{0.67}Cu_{0.08}Ti_{0.25}$, which could provide improved heat resistance and high temperature strength. Sintering the Ti-Al-W powders allowed obtaining phases such as γ-TiAl, Al_2Ti, and W.

The above-disclosed results show potential of the EEW for producing micro/nano alloy particle mixtures from intertwisted wires of at least three dissimilar metal wires. It is worth noting, however, that further research is needed for establishing relashionships between:

- $E/\sum E_s$ parameter and particle size distribution as well as phase formation;
- Particle size distribution, phase composition, sintering temperature, time and microstructures, as well as physico-mechanical characteristics of the samples sintered.

Obtaining these data is necessary for fabrication of feedstocks from micro/nano powders Ti-Al-M alloy powders.

Declaration of Competing Interest

None.

Acknowledgment

This work was carried out with funding from Russian Science Fund project No. 21-79-30006.

References

[1] K. Rane, M. Strano, A comprehensive review of extrusion-based additive manufacturing processes for rapid production of metallic and ceramic parts, Adv. Manuf. 7 (2019) 155–173, https://doi.org/10.1007/s40436-019-00253-6.
[2] Aghnia Ilmiah Nurhudan, Sugeng Supriadi, Yudan Whulanza, Agung Shamsuddin Saragih, Additive manufacturing of metallic based on extrusion process: A review, J. Manuf. Process. 66 (2021) 228–237, https://doi.org/10.1016/j.jmapro.2021.04.018.
[3] Joaquim Manoel Justino Netto, Henrique Takashi Idogava, Luiz Eduardo Frezzatto Santos, Zilda de Castro Silveira, Pedro Romio, Jorge Lino Alves, Screw-assisted 3D printing with granulated materials: a systematic review, Int. J. Adv. Manuf. Technol. 115 (2021) 2711–2727, https://doi.org/10.1007/s00170-021-07365-z.
[4] Gurminder Singha, Jean-Michel Missiae, Didier Bouvard, Jean-Marc Chaix, Additive manufacturing of 17–4 PH steel using metal injection molding feedstock: analysis of 3D extrusion printing, debinding and sintering, Additive Manufact. 47 (2021) 102287. https://doi.org/10.1016/j.addma.2021.102287.
[5] Ali Dehghan-Manshadi, Yu Peng, Matthew Dargusch, David StJohn, Ma Qian, Metal injection moulding of surgical tools, biomaterials and medical devices: A review, Powder Technol. 364 (2020) 189–204, https://doi.org/10.1016/j.powtec.2020.01.073.
[6] G. Singh, J.M. Missiaen, D. Bouvard, J.M. Chaix, Copper extrusion 3D printing using metal injection moulding feedstock: analysis of process parameters for green density and surface roughness optimization, Addit. Manuf. 38 (2021) 101778. https://doi.org/10.1016/j.addma.2020.101778.
[7] T. Rosnitschek, A. Seefeldt, B. Alber-Laukant, T. Neumeyer, V. Altstädt, S. Tremmel, Correlations of geometry and infill degree of extrusion additively manufactured 316L stainless steel components, Materials. 14 (2021) 5173, https://doi.org/10.3390/ma14185173.
[8] A.S. Vishwanath, K. Rane, J. Schaper, M. Strano, R. Casati, Rapid production of AZ91 Mg alloy by extrusion based additive manufacturing process, Powder Metall. (2021) 370–377, https://doi.org/10.1080/00325899.2021.1911457.
[9] Q. He, J. Jiang, X. Yang, L. Zhang, Z. Zhou, Y. Zhong, Z. Shen, Additive manufacturing of dense zirconia ceramics by fused deposition modeling via screw extrusion, J. Eur. Ceram. Soc. 41 (2021) 1033, https://doi.org/10.1016/j.jeurceramsoc.2020.09.018.
[10] W. Lengauer, I. Duretek, M. Fürst, V. Schwarz, J. Gonzalez-Gutierrez, S. Schuschnigg, C. Kukla, M. Kitzmantel, E. Neubauer, C. Lieberwirth, V. Morrison, Fabrication and properties of extrusion-based 3D-printed hardmetal and cermet components, Int. J. Refract. Met. Hard Mater. 82 (2019) 141–149, https://doi.org/10.1016/j.ijrmhm.2019.04.011.
[11] Qu Zhu Baojun, Tao Ying Xuanhui, Powder injection molding of WC–8% Co tungsten cemented carbide, Int. J. Refract. Met. Hard Mater. 20 (2002) 389–394, https://doi.org/10.1016/S0263-4368(02)00015-X.
[12] O. Ghanmi, V. Demers, Molding properties of titanium-based feedstock used in low-pressure powder injection molding, Powder Technol. 379 (2021) 515–525, https://doi.org/10.1016/j.powtec.2020.10.068.
[13] D.M. Krotov, Possibilities and problems of using MIM technology in manufacturing parts of aircraft elements made of titanium and titanium alloys, AIP Conference Proceedings, 2318, 2021, 020002. https://doi.org/10.1063/5.0037321.
[14] Masoud Shahidi Moghadam, Abdolali Fayyaz, Mohammad Ardestani, Fabrication of titanium components by low-pressure powder injection moulding using hydride-dehydride titanium powder, Powder Technol. 377 (2021) 70–79, https://doi.org/10.1016/j.powtec.2020.08.075.
[15] Raphaël Côté, Mohamed Azzouni, Vincent Demers, Impact of binder constituents on the moldability of titanium-based feedstocks used in low-pressure powder injection molding, Powder Technol. 381 (2021) 255–268, https://doi.org/10.1016/j.powtec.2020.12.008.
[16] Jin-Woong Lee, Suman Timilsina, Gi-Woo Kim, Ji Sik Kim, A new strategy for novel binder discovery in nano and μ powder injection molding: A metaheuristics-assisted virtual combinatorial materials search, Powder Technol. 302 (2016) 187–195, https://doi.org/10.1016/j.powtec.2016.08.055.
[17] Oh. Joo Won, Won Sik Lee, Seong Jin Park, Influence of nano powder on rheological behavior of bimodal feedstock in powder injection molding, Powder Technol. 311 (2017) 18–24, https://doi.org/10.1016/j.powtec.2017.01.081.
[18] Swathi K. Manchili, Eduard Hryha JohanWendel, Lars Nyborg, Sintering of bimodal micrometre/nanometre iron powder compacts - A master sintering curve approach, Powder Technol. 391 (2021) 557–568, https://doi.org/10.1016/j.powtec.2021.06.052.
[19] V.M. Romanova, G.V. Ivanenkov, A.R. Mingaleev, A.E. Ter-Oganesyan, T.A. Shelkovenko, S.A. Pikuz, Electric explosion of fine wires: three groups of materials, Plasma Phys. Rep. 41 (2015) 617–636, https://doi.org/10.1134/S1063780X15080085.
[20] Yu.A. Kotov, The electrical explosion of wire: A method for the synthesis of weakly aggregated nanopowders, Nanotechnol. Russia. 4 (2009) 415–424, https://doi.org/10.1134/S1995078009070039.
[21] A.V. Pervikov, Metal, metal composite, and composited nanoparticles obtained by electrical explosion of wires, Nanobiotechnol. Rep. 16 (2021) 401–420, https://doi.org/10.1134/S2635167621040091.
[22] M.I. Lerner, A.V. Pervikov, E.A. Glazkova, N.G. Rodkevich, N.E. Toropkov, Electrical explosion synthesis, oxidation and sintering behavior of Ti-Al intermetallide powders, Metals. 11 (2021) 760, https://doi.org/10.3390/met11050760.
[23] A.V. Pervikov, E.A. Glazkova, M.I. Lerner, Energy characteristics of the electrical explosion of two intertwined wires made of dissimilar metals, Phys. Plasmas. 25 (2018) 070701. https://doi.org/10.1063/1.5034184.

[24] A.V. Pervikov, K.V. Suliz, M.I. Lerner, Nanoalloying of clusters of immiscible metals and the formation of bimetallic nanoparticles in the conditions of non-synchronous explosion of two wires, Powder Technol. 360 (2020) 855–862, https://doi.org/10.1016/j.powtec.2019.11.003.
[25] A.V. Pervikov, S.O. Kazantsev, A.S. Lozhkomoev, M.I. Lerner, Bimetallic Al-Ag, Al-cu and Al-Zn nanoparticles with controllable phase compositions prepared by the electrical explosion of two wires, Powder Technol. 372 (2020) 136–147, https://doi.org/10.1016/j.powtec.2020.05.088.
[26] H.P. Lim, W.Y.H. Liew, G.J.H. Melvin, Z.-T. Jiang, A short review on the phase structures, oxidation kinetics, and mechanical properties of complex Ti-Al alloys, Materials. 14 (2021) 1677, https://doi.org/10.3390/ma14071677.
[27] Zhanqi Liu, Chenyang Wang, Wenbo Wang, Xu Guojian, Xiangyu Liu, Effects of tantalum on the microstructure and properties of Ti-48Al-2Cr-2Nb alloy fabricated via laser additive manufacturing, Mater. Charact. 179 (2021) 111317. https://doi.org/10.1016/j.matchar.2021.111317.
[28] Shili Shu, Feng Qiu, Cunzhu Tong, Xiaonan Shan, Qichuan Jiang, Effects of Fe, co and Ni elements on the ductility of TiAl alloy, J. Alloys Compd. 617 (2014) 302–305, https://doi.org/10.1016/j.jallcom.2014.07.199.
[29] S. Jyotsna Gupta, S. Aravindan Ghosh, Effect of Mo and space holder content on microstructure, mechanical and corrosion properties in Ti6AlxMo based alloy for bone implant, Mater. Sci. Eng. C. 123 (2021) 111962. https://doi.org/10.1016/j.msec.2021.111962.
[30] A.V. Bakulin, S.S. Kulkov, S.E. Kulkova, Diffusion properties of oxygen in the α2-Ti3Al alloy, Intermetallics. 137 (2021) 107281. https://doi.org/10.1016/j.intermet.2021.107281.
[31] D.V. Lazurenko, I.A. Bataev, V.I. Mali, A.M. Jorge Jr., A. Stark, F. Pyczak, T.S. Ogneva, I.N. Maliutina, Synthesis of metal-intermetallic laminate (MIL) composites with modified Al3Ti structure and in situ synchrotron X-ray diffraction analysis of sintering process, Mater. Des. 151 (2018) 8–16, https://doi.org/10.1016/j.matdes.2018.04.038.
[32] Ruoyu Han, Wu Jiawei, Haibin Zhou, Weidong Ding, Aici Qiu, Thomas Clayson, Yanan Wang, Hang Ren, Characteristics of exploding metal wires in water with three discharge types, J. Appl. Phys. 122 (2017) 033302. https://doi.org/10.1063/1.4994009.
[33] G.S. Sarkisov, P.V. Sasorov, K.W. Struve, D.H. McDaniel, State of the metal core in nanosecond exploding wires and related phenomena, J. Appl. Phys. 96 (2004) 1674–1686, https://doi.org/10.1063/1.1767976.
[34] S.I. Tkachenko, A.R. Mingaleev, V.M. Romanova, A.E. Ter-Oganes'yan, T.A. Shelkovenko, S.A. Pikuz, Distribution of matter in the current - carrying plasma and dense core of the discharge channel formed upon electrical wire explosion, Plasma Phys. Rep. 35 (2009) 734–753, https://doi.org/10.1134/S1063780X09090037.
[35] Xiaoping Liu, Kai You, Zhenxia Wang, Minquan Zhang, Zhiyong He, Effect of Mo-alloyed layer on oxidation behavior of TiAl-based alloy, Vacuum. 89 (2013) 209–214, https://doi.org/10.1016/j.vacuum.2012.05.015.
[36] Tian Shiwei, He Anrui, Liu Jianhua, Zhang Yefei, Yang Yonggang, Zhang Yun, Jiang Haitao, Oxidation resistance of TiAl alloy improved by hot-pack rolling and cyclic heat treatment, Mater. Charact. 178 (2021) 111196. https://doi.org/10.1016/j.matchar.2021.111196.
[37] R.B. Baksht, S.I. Tkachenko, V.M. Romanova, A.R. Mingaleev, V.I. Oreshkin, A.E. Ter-Oganes'yan, T.A. Khattatov, T.A. Shelkovenko, S.A. Pikuz, Stratification dynamics and the development of electrothermal instability at the wire explosion, Tech. Phys. 58 (2013) 1129–1137, https://doi.org/10.1134/S1063784213080021.
[38] V.M. Romanova, G.V. Ivanenkov, A.R. Mingaleev, A.E. Ter-Oganesyan, I.N. Tilikin, T.A. Shelkovenko, S.A. Pikuz, On the phase state of thin silver wire cores during a fast electric explosion, Phys. Plasmas. 25 (2018) 112704. https://doi.org/10.1063/1.5052549.
[39] V.M. Romanova, G.V. Ivanenkov, E.V. Parkevich, I.N. Tilikin, M.A. Medvedev, T.A. Shelkovenko, S.A. Pikuz, A.S. Selyukov, Laser scattering by submicron droplets formed during the electrical explosion of thin metal wires, J. Phys. D. Appl. Phys. 54 (2021) 175201. https://doi.org/10.1088/1361-6463/abdce5.
[40] B. Bora, S.S. Kausik, C.S. Wong, O.H. Chin, S.L. Yap, L. Soto, Observation of the partial reheating of the metallic vapor during the wire explosion process for nanoparticle synthesis, Appl. Phys. Lett. 104 (2014) 223108. https://doi.org/10.1063/1.4881838.
[41] L. Prem Ranjan, Santhosh Kumar, H. Suematsu, S.R. Chakravarthy, R. Jayaganthan, R. Sarathi, Thermodynamic analysis of ZnO nanoparticle formation by wire explosion process and characterization, Ceram. Int. 43 (2017) 6709–6720, https://doi.org/10.1016/j.ceramint.2017.02.069.
[42] Huantong Shi, Wu Jian, Xingwen Li, A.B. Murphy, Xudong Li, Chen Li, Penghui Li, Understanding the nanoparticle formation during electrical wire explosion using a modified moment model, Plasma Sources Sci. Technol. 28 (2018) 085010. https://doi.org/10.1088/1361-6595/ab216f.
[43] K.B. Abramova, N.A. Zlatin, B.P. Peregud, Magnetohydrodynamic instability of liquid and solid conductors. Destruction of conductors by an electric current, JETP. 42 (1975) 1019. http://www.jetp.ras.ru/cgi-bin/dn/e_042_06_1019.pdf.
[44] V.V. Apollonov, N.V. Pletnev, Formation of extended directional breakdown channels produced by a copper wire exploding in the atmosphere, Tech. Phys. 58 (2013) 1770–1782, https://doi.org/10.1134/S1063784213120049.
[45] P. Mossino, Some aspects in self-propagating high-temperature synthesis, Ceram. Int. 30 (2004) 311–332, https://doi.org/10.1016/S0272-8842(03)00119-6.
[46] A. Pervikov, N. Toropkov, S. Kazantsev, O. Bakina, E. Glazkova, M. Lerner, Preparation of nano/micro bimodal aluminum powder by electrical explosion of wires, Materials. 14 (2021) 6602, https://doi.org/10.3390/ma14216602.
[47] B.M. Smirnov, Processes involving clusters and small particles in a buffer gas, Physics-Uspekhi 54 (2011) 691–721, https://doi.org/10.3367/UFNe.0181.201107b.0713.
[48] A. Dębski, R. Dębski, W. Gąsior, New features of Entall database: comparison of experimental and model formation enthalpies, Arch. Metall. Mater. 59 (4) (2014) 1337–1343, https://doi.org/10.2478/amm-2014-0228.
[49] J.J.S. Dilip, H. Miyanaji, Austin Lassell, Thomas L. Starr, Brent Stucker, A novel method to fabricate TiAl intermetallic alloy 3D parts using additive manufacturing, Def. Technol. 13 (2017) 72–76, https://doi.org/10.1016/j.dt.2016.08.001.
[50] Chang Kyu Kim, Gyoung-ja Lee, min Ku Lee, Chang Kyu Rhee. A novel method to prepare cu@ag core–shell nanoparticles for printed flexible electronics, Powder Technol. 263 (2014) 1–6, https://doi.org/10.1016/j.powtec.2014.04.064.
[51] Fu-Sheng Sun, Chun-Xiao Cao, Ming-Gao Yan, Seung-Eon Kim, Yong-Tailee, Alloying mechanism of beta stabilizers in a TiAl alloy, Metall. Mater. Trans. A 32 (2001) 1573–1589, https://doi.org/10.1007/s11661-001-0136-4.
[52] Xiaobing Li, Hongjian Tang, Weiwei Xing, Pengxiang Zhao, Bo Chen, Yingche Ma, Kui Liu, Microstructural stability, phase evolution and mechanical properties of a forged W-modified high-Mn β-γ-TiAl alloy, Intermetallics. 136 (2021) 107230. https://doi.org/10.1016/j.intermet.2021.107230.